

# A chiral quark-soliton model with broken scale invariance for nuclear matter

Alessandro Drago and Mantovani Sarti Valentina

*Dipartimento di Fisica, Università di Ferrara and INFN, Sez. Ferrara, 44100 Ferrara, Italy*

We present a model for describing nuclear matter at finite density based on quarks interacting with chiral fields,  $\sigma$  and  $\pi$  and with vector mesons introduced as massive gauge fields. The chiral Lagrangian includes a logarithmic potential, associated with the breaking of scale invariance. We provide results for the soliton in vacuum and at finite density, using the Wigner-Seitz approximation. We show that the model can reach higher densities respect to the linear- $\sigma$  model and that the introduction of vector mesons allows to obtain saturation. This result was never obtained before in similar approaches.

PACS numbers: 12.39.Fe, 21.65.Mn, 21.30.Fe

## I. INTRODUCTION

The problem of studying nuclear matter with chiral Lagrangians is not trivial; for instance models based on the linear  $\sigma$ -model fail to describe nuclear matter already at  $\rho \sim \rho_0$  because the normal solution in which chiral symmetry is broken becomes unstable respect to the Lee-Wick phase. In Ref. [1] Furnstahl and Serot conclude that the failure of the  $\sigma$ -model is due to the restrictions on the scalar field dynamics imposed by the Mexican hat potential. A possible solution to this problem is still to use a linear realization, but with a new potential, which includes terms not present in the Mexican hat potential. A guideline in building such a potential is scale invariance [2–5].

In QCD the invariance under dilatation is spontaneously broken due to the presence of the parameter  $\Lambda_{QCD}$  coming from the renormalization process. Formally, the non conservation of the dilatation current is strictly connected to a not vanishing gluon condensate:

$$\langle \partial_\mu j_{QCD}^\mu \rangle = \frac{\beta(g)}{2g} \langle F_{\mu\nu}^a(x) F^{a\mu\nu}(x) \rangle. \quad (1)$$

In the approach of Schechter [6], and of Migdal and Shifman [7] a scalar field representing the gluon condensate is introduced and its dynamics is regulated by a potential chosen so that it reproduces (at Mean-Field level) the divergence of the scale current that in QCD is given by Eq. (1). The potential of the dilaton field is therefore determined by the equation:

$$\theta_\mu^\mu = 4V(\phi) - \phi \frac{\partial V}{\partial \phi} = 4\epsilon_{vac} \left( \frac{\phi}{\phi_0} \right)^4 \quad (2)$$

where the parameter  $\epsilon_{vac}$  represents the vacuum energy. To take into account massless quarks a generalization was proposed in Ref. [8], so that also chiral fields contribute to the trace anomaly. In this way the single scalar field of Eq. (2) is replaced by a set of scalar and pseudoscalar fields  $\{\sigma, \pi, \phi\}$ .

It has already been shown that an hadronic model based on this dynamics provides a good description of nuclear physics at densities about  $\rho_0$  and it describes the

gradual restoration of chiral symmetry at higher densities [9]. In the same work the authors have shown a phase diagram, where the interplay between chiral and scale invariance restoration lead to a scenario similar to that proposed by McLerran and Pisarski in [10]. This is not too surprising since the large  $N_c$  limit explored in [10] should be well represented in chiral models as the one discussed in [9]. It is therefore tempting to explore the scenario presented in [9] at a more microscopic level.

*The new idea we develop in this work is to interpret the fermions as quarks, to build the hadrons as solitonic solutions of the fields equations as in [11, 12] and, finally, to explore the properties of the soliton at finite density using the Wigner-Seitz approximation.*

Similar approaches to a finite density system have been investigated in the past [13–19]. A problem of those works is that the solitonic solutions are unstable and disappear already at moderate densities when e.g. the linear  $\sigma$ -model is adopted [18]. We are therefore facing an instability similar to the one discussed and solved when studying nuclear matter with hadronic chiral Lagrangians. The first aim of our work is *to check whether the inclusion of the logarithmic potential allows the soliton crystal to reach higher densities*. The second and more important aim is *to check whether the inclusion of vector mesons in the dynamics of the quarks can provide saturation for chiral matter*.

We should remark that the version of this model without vector mesons has already been studied at zero density in [20], but using a different technique to describe the single nucleon. Instead no calculation exists with the vector mesons. Moreover, both versions of the model are unexplored at finite density.

The structure of the paper is as follows. In Sec. II we describe the model we are using, in Sec. III we review the Mean-Field approximation and the hedgehog ansatz while in Sec. IV we present the technique adopted for projection. Later in Sec. V we describe the Wigner-Seitz approximation used to mimic a system at finite density. Next in Sec. VI and in Sec. VII we present our results, firstly for the soliton in vacuum both at Mean-Field level and by adopting a projection technique and then we show the results for the Wigner-Seitz lattice of solitons. Fi-

nally, in Sec. VIII we present our conclusions and future outlooks.

## II. THE MODEL

In a chiral quark-soliton model quarks are coupled to mesons in a chirally invariant way. Following Refs. [2–5, 9] we consider the Lagrangian:

$$\begin{aligned}\mathcal{L}_0 = & \bar{\psi}(i\gamma^\mu\partial_\mu - g_\pi(\sigma + i\boldsymbol{\pi} \cdot \boldsymbol{\tau}\gamma_5))\psi \\ & + \frac{1}{2}(\partial_\mu\phi\partial^\mu\phi + \partial_\mu\sigma\partial^\mu\sigma + \partial_\mu\boldsymbol{\pi} \cdot \partial^\mu\boldsymbol{\pi}) \\ & - V(\phi, \sigma, \pi).\end{aligned}\quad (3)$$

Here  $\psi$  is the quark field,  $\sigma$  and  $\pi$  are the chiral fields and  $\phi$  is the dilaton field which, in the present calculation, is kept frozen at its vacuum value  $\phi_0$ .

An extension of this model, already discussed in Refs. [2–5, 9], is to add the dynamics of vector mesons and to incorporate the idea of universal coupling [21]. This can be achieved by considering the vector mesons as massive gauge fields, following also the scheme of Ref. [22]. The new Lagrangian is given by:

$$\begin{aligned}\mathcal{L}_{VM} = & \bar{\psi}(i\gamma^\mu\partial_\mu - g_\pi(\sigma + i\boldsymbol{\pi} \cdot \boldsymbol{\tau}\gamma_5) + g_\rho\gamma^\mu\frac{\boldsymbol{\tau}}{2} \cdot (\boldsymbol{\rho}_\mu + \gamma_5\mathbf{A}_\mu) \\ & - \frac{g_\omega}{3}\gamma^\mu\omega_\mu)\psi + \frac{\beta}{2}(D_\mu\sigma D^\mu\sigma + D_\mu\boldsymbol{\pi} \cdot D^\mu\boldsymbol{\pi}) \\ & - \frac{1}{4}(\boldsymbol{\rho}_{\mu\nu} \cdot \boldsymbol{\rho}^{\mu\nu} + \mathbf{A}_{\mu\nu} \cdot \mathbf{A}^{\mu\nu} + \omega_{\mu\nu}\omega^{\mu\nu}) \\ & + \frac{1}{2}m_\rho^2(\boldsymbol{\rho}_\mu \cdot \boldsymbol{\rho}^\mu + \mathbf{A}_\mu \cdot \mathbf{A}^\mu) + \frac{1}{2}m_\omega^2\omega_\mu\omega^\mu \\ & - V(\phi_0, \sigma, \pi)\end{aligned}\quad (4)$$

where  $\omega_\mu$  is a vector-isoscalar coupled to baryon current,  $\boldsymbol{\rho}_\mu$  and  $\mathbf{A}_\mu$  are respectively a vector-isovector and an axial-vector-isovector fields coupled to isospin and axial-vector current. The covariant derivatives for the chiral fields and the field tensors for vector mesons read:

$$\begin{aligned}D_\mu\sigma &= \partial_\mu\sigma + g_\rho\mathbf{A}_\mu \cdot \boldsymbol{\pi}, \\ D_\mu\boldsymbol{\pi} &= \partial_\mu\boldsymbol{\pi} + g_\rho(\boldsymbol{\rho}_\mu \wedge \boldsymbol{\pi} - \mathbf{A}_\mu\sigma), \\ \omega_{\mu\nu} &= \partial_\mu\omega_\nu - \partial_\nu\omega_\mu, \\ \boldsymbol{\rho}_{\mu\nu} &= \partial_\mu\boldsymbol{\rho}_\nu - \partial_\nu\boldsymbol{\rho}_\mu + g_\rho(\boldsymbol{\rho}_\mu \wedge \boldsymbol{\rho}_\nu + \mathbf{A}_\mu \wedge \mathbf{A}_\nu), \\ \mathbf{A}_{\mu\nu} &= \partial_\mu\mathbf{A}_\nu - \partial_\nu\mathbf{A}_\mu + g_\rho(\boldsymbol{\rho}_\mu \wedge \mathbf{A}_\nu + \mathbf{A}_\mu \wedge \boldsymbol{\rho}_\nu).\end{aligned}\quad (5)$$

The pion field mixes with the longitudinal component of the  $a_1$  [23, 24] and so to ensure that the pion gets its physical mass once the two fields are decoupled, we need to introduce the constant:

$$\beta = \frac{m_\rho^2}{m_\rho^2 - g_\rho^2 f_\pi^2}.\quad (6)$$

The potential is given by:

$$\begin{aligned}V(\phi, \sigma, \pi) = & B\phi_0^4 \left( \ln \frac{\phi}{\phi_0} - \frac{1}{4} \right) - \frac{1}{2}B\delta\phi^4 \ln \frac{\sigma^2 + \boldsymbol{\pi}^2}{\sigma_0^2} \\ & + \frac{1}{2}B\delta\phi^2 \frac{\phi_0^2}{\sigma_0^2} \left( \sigma^2 + \boldsymbol{\pi}^2 - \phi^2 \frac{\sigma_0^2}{2\phi_0^2} \right) \\ & - \frac{1}{4}\epsilon_1 \left( \frac{\phi}{\phi_0} \right)^2 \left[ \frac{4\sigma}{\sigma_0} - 2 \left( \frac{\sigma^2 + \boldsymbol{\pi}^2}{\sigma_0^2} \right) - \left( \frac{\phi}{\phi_0} \right)^2 \right] - V_0\end{aligned}\quad (7)$$

where the logarithmic term generates from (2). The first two terms of the potential are responsible for the breaking of scale invariance, while the second line is needed to ensure that in the vacuum  $\phi = \phi_0$ ,  $\sigma = \sigma_0$  and  $\boldsymbol{\pi} = 0$ , i.e it provides spontaneous symmetry breaking. The last line explicitly breaks the chiral invariance of the lagrangian, giving mass to the pion.

In this work we assign the following values to the masses of bare fields:  $m_\pi = 139$  MeV,  $m_\rho = m_A = 776$  MeV and  $m_\omega = 782$  MeV. For the sigma field, since there are no experimental constraints, we use  $m_\sigma = 550$  MeV and  $m_\sigma = 1200$  MeV which are typical values used in nuclear physics if the sigma has to provide the intermediate range attraction. We relate the quark-omega and the quark-rho couplings to the corresponding couplings with the nucleons. We keep fixed  $g_\rho = 4$  and we vary  $g_\omega$  between 10 and 13. The pion-quark coupling constant  $g_\pi$  will vary from 3.9 to 5. By varying the coupling constants in the ranges indicated above we will be able to tune the attractive and the repulsive interactions, in order to obtain saturation when studying the total energy of the soliton at finite density. The constants  $B$  and  $\phi_0$  can be fixed by choosing a value for the mass of the glueball and for the vacuum energy  $\epsilon_{vac}$ , while  $\delta = 4/33$  is provided by the QCD beta function and it corresponds to the relative weight of the fermionic and of the gluonic degrees of freedom. Finally the constant  $V_0$  ensures that the potential energy is vanishing in the vacuum.

As anticipated, we choose to keep the dilaton field frozen. This decision (which obviously simplifies the dynamics of the system) can be justified by the results obtained in [3, 9], where it has been shown that at low temperatures the dilaton remains close to its vacuum value even at large densities. Therefore the degrees of freedom of our model are limited to quarks, chiral fields and vector mesons, similarly to the linear  $\sigma$ -model whose solitonic solutions have been obtained in [11, 22]. The potential can be written in a simpler form and it reads:

$$V(\sigma, \pi) = \lambda_1^2(\sigma^2 + \boldsymbol{\pi}^2) - \lambda_2^2 \ln(\sigma^2 + \boldsymbol{\pi}^2) - \sigma_0 m_\pi^2 \sigma \quad (8)$$

where:

$$\lambda_1^2 = \frac{1}{2} \frac{B\delta\phi_0^4 + \epsilon_1}{\sigma_0^2} = \frac{1}{4}(m_\sigma^2 + m_\pi^2) \quad (9)$$

$$\lambda_2^2 = \frac{1}{2}B\delta\phi_0^4 = \frac{\sigma_0^2}{4}(m_\sigma^2 - m_\pi^2) \quad (10)$$

$$\epsilon_1 = m_\pi^2 \sigma_0^2. \quad (11)$$

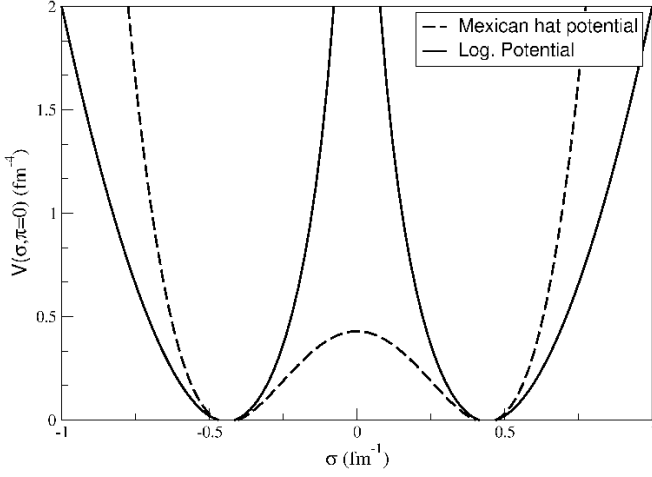


Figure 1. Comparison between the logarithmic (solid line) and the Mexican hat potential (dashed line).

Here the vacuum value  $\sigma_0$  is fixed to be equal to  $f_\pi = 93$  MeV.

It is interesting to compare the logarithmic with the Mexican hat potential. In Fig. 1 it can be seen that in the case of the Mexican hat potential it is relatively easy to restore chiral symmetry by climbing the maximum located at the center. This is not possible in the case of the logarithmic potential as long as the dilaton field remains frozen. Since only at large temperatures the dilaton field changes significantly [9] we can expect that at large densities and moderate temperatures this model provides more stable solitonic solutions. This is a crucial question which will be investigated in our paper.

An important point in our approach is that we aim at describing the dynamics of nuclear matter by incorporating all the interactions already at a quark level. This is at variance with e.g. the approach of Ref.[25, 26] where the vector field  $\omega$  was introduced only at the nucleon level, but was not present in the dynamics of the quarks.

### III. MEAN-FIELD AND HEDGEHOG ANSATZ

The Euler-Lagrangian equations that follow from the Lagrangian given in eq. (4) read:

$$\begin{aligned}
 [i\cancel{D} - g_\pi(\sigma + i\boldsymbol{\pi} \cdot \boldsymbol{\tau}\gamma_5) + g_\rho\frac{\boldsymbol{\tau}}{2} \cdot (\boldsymbol{\rho} + \gamma_5\boldsymbol{A}) - \frac{g_\omega}{3}\cancel{\phi}]\psi &= 0, \\
 \beta\partial_\mu D^\mu\sigma &= -\beta g_\rho\boldsymbol{A}_\mu \cdot \boldsymbol{\pi} - g\bar{\psi}\psi - \frac{\partial V}{\partial\sigma}, \\
 \beta\partial_\mu D^\mu\boldsymbol{\pi} &= \beta g_\rho(-\boldsymbol{\rho}_\mu \times D^\mu\boldsymbol{\pi} + \boldsymbol{A}_\mu D^\mu\sigma) - ig\bar{\psi}\boldsymbol{\tau}\gamma_5\psi - \frac{\partial V}{\partial\boldsymbol{\pi}}, \\
 -\partial^\mu\boldsymbol{\rho}_{\mu\nu} &= g_\rho\boldsymbol{v}_\nu + m_\rho^2\boldsymbol{\rho}_\nu, \\
 -\partial^\mu\boldsymbol{A}_{\mu\nu} &= g_\rho\boldsymbol{a}_\nu + m_\rho^2\boldsymbol{A}_\nu, \\
 -\partial^\mu\omega_{\mu\nu} &= -\frac{1}{3}g_\omega\bar{\psi}\gamma_\nu\psi + m_\omega^2\omega_\nu.
 \end{aligned} \tag{12}$$

Here  $\boldsymbol{v}_\nu$  and  $\boldsymbol{a}_\nu$  are the vector and the axial-vector currents:

$$\boldsymbol{v}_\nu = \boldsymbol{\rho}_\mu \times \boldsymbol{\rho}_{\mu\nu} + \boldsymbol{A}_\mu \times \boldsymbol{A}_{\mu\nu} + \beta\boldsymbol{\pi} \times D^\nu\boldsymbol{\pi} + \bar{\psi}\gamma_\nu\frac{\boldsymbol{\tau}}{2}\psi, \tag{13}$$

$$\begin{aligned}
 \boldsymbol{a}_\nu &= \boldsymbol{\rho}_\mu \times \boldsymbol{A}_{\mu\nu} + \boldsymbol{A}_\mu \times \boldsymbol{\rho}_{\mu\nu} + \beta\boldsymbol{\pi} \times D^\nu\boldsymbol{\sigma} - \beta\sigma D_\nu\boldsymbol{\pi} \\
 &\quad + \bar{\psi}\gamma_5\gamma_\nu\frac{\boldsymbol{\tau}}{2}\psi.
 \end{aligned} \tag{14}$$

The fields equations for the model without vector mesons, provided by the Lagrangian in eq. (3), can be obtained by the previous ones by fixing  $g_\rho = g_\omega = 0$ .

The previous equations are relations between quantum fields. The starting point of our calculation is the Mean-Field approximation, where mesons are described by time-independent, classical fields and where powers and products of these fields are replaced by powers and products of their expectation values. The quark spinor in the spin-isospin space is:

$$\psi = \frac{1}{\sqrt{4\pi}} \begin{pmatrix} u(r) \\ iv(r)\boldsymbol{\sigma} \cdot \hat{\boldsymbol{r}} \end{pmatrix} \chi_h \tag{15}$$

where the spinor  $\chi_h$ , defined as:

$$\chi_h = \frac{1}{\sqrt{2}}(|u_\downarrow\rangle - |d_\uparrow\rangle) \tag{16}$$

satisfies the condition for the Grand Spin  $\boldsymbol{G} = \boldsymbol{I} + \boldsymbol{J}$ :

$$\boldsymbol{G}\chi_h = 0. \tag{17}$$

The hedgehog baryon  $|B\rangle = |N_c q\rangle|\sigma\rangle|\pi\rangle|\omega\rangle|\rho\rangle|A\rangle$  is given by the product of quarks and coherent states of mesons fields and it corresponds to a linear combination of states with  $I = 1/2$  and  $I = 3/2$ :

$$|B\rangle = \sum_{JMM_I} (-)^{J+M} C_J \delta_{M, -M_I} |J = I, M = -I_3, M_I\rangle. \tag{18}$$

An explicit expression for the coefficients  $C_J$  will be given in Sec. IV.

It can be shown that the hedgehog state is one element of an infinite class of degenerate solutions of field equations at Mean-Field level [27]. The profiles of the chiral and the vector mesons fields in the hedgehog state are given by the relations:

$$\begin{aligned}
 \frac{\langle B|\sigma|B\rangle}{\langle B|B\rangle} &= \sigma_h(r), & \frac{\langle B|\boldsymbol{\pi}_a|B\rangle}{\langle B|B\rangle} &= \hat{r}_a h(r) \\
 \frac{\langle B|\omega_\mu|B\rangle}{\langle B|B\rangle} \omega_0(r) &= \omega(r) \\
 \frac{\langle B|\boldsymbol{\rho}_a|B\rangle}{\langle B|B\rangle} &= \rho_i^a(r) = \rho(r)\epsilon^{ika}\hat{r}^k \\
 \frac{\langle B|\boldsymbol{A}_a|B\rangle}{\langle B|B\rangle} &= A_i^a(r) = A_S(r)\delta^{ai} + A_T(r)(\hat{r}^a\hat{r}^i - \frac{1}{3}\delta^{ai})
 \end{aligned}$$

At Mean-Field level the mesons fields are classical and the differential equations governing their dynamics have to be supplemented by the appropriate boundary conditions. For the single nucleon case we impose the following boundary conditions to the fields:

$$\begin{aligned} u'(0) &= v(0) = 0, \\ \sigma'_h(0) &= h(0) = 0, \\ \rho(0) &= \omega'(0) = A'_S(0) = A_T(0) = 0, \end{aligned} \quad (19)$$

while at infinity the boundary conditions read:

$$\begin{aligned} \sigma_h(\infty) &= \sigma_0, \quad h(\infty) = 0, \\ \frac{v(\infty)}{u(\infty)} &= \sqrt{\frac{-g\sigma_0 + \varepsilon}{-g\sigma_0 - \varepsilon}}, \\ \omega'(\infty) &= \rho'(\infty) = A'_S(\infty) = A'_T(\infty) = 0, \end{aligned} \quad (20)$$

where  $\varepsilon$  is the quark eigenvalue.

The total energy of the soliton at Mean-Field level is given by:

$$\begin{aligned} E_{MFA} &= 4\pi \int r^2 dr (E_{int} + E_{kin,Q} + E_\sigma + E_\pi \\ &\quad + E_\omega + E_\rho + E_A + E_{pot}) \end{aligned} \quad (21)$$

where explicit expressions for each term in the energy density can be found in Appendix I. A test of the numerical accuracy of the solution originates from another way of expressing the energy, obtained by Rafelski [28] by integrating out the fermionic fields:

$$\begin{aligned} E_{Raf.} &= \int d^3r \left[ 4 \left( V - \sigma \frac{\partial V}{\partial \sigma} - \pi \frac{\partial V}{\partial \pi} \right) - m_\omega^2 \omega^2 \right. \\ &\quad \left. + m_\rho^2 \left( 2\rho^2 + 3A_S^2 + \frac{2}{3}A_T^2 \right) \right] \end{aligned} \quad (22)$$

Our solutions satisfy this consistency test up to a precision of the order of  $10^{-3}$ .

#### IV. PROJECTION

The hedgehog baryon defined in section III is not an eigenstate of isospin and angular momentum. Moreover this semi-classical solution also breaks the translational symmetry of the Lagrangian, since the localized soliton is not an eigenstate of the linear momentum, either. In this work we restore the invariance under rotations by using the projection technique developed in [11, 29]. Instead, we will not restore the translational invariance of our soliton. The spin-isospin eigenstates are defined as follows:

$$|JMM_I\rangle = N_{JM_I} \int d^3\Omega D_{M,-M_I}^J(\Omega)^* \hat{R}(\Omega)|B\rangle \quad (23)$$

where the weight functions  $D$  are the Wigner functions,  $\hat{R}(\Omega)$  is a spatial rotation through Euler angles

$\Omega \equiv (\alpha, \beta, \gamma)$  and  $N_{JM_I}$  is a normalization factor.

Since the hedgehog states are eigenstates of the Grand Spin  $\mathbf{G}$ , it is equivalent to rotate either in spin or in isospin space. Moreover, when studying diagonal matrix elements of nucleon states, it is customary to work with states where the third component of the angular momentum  $M$  is equal to  $-M_I$  since in this case the expression of the Wigner function is particularly simple. In this way the projection operator becomes:

$$P_{JM} = \frac{2J+1}{8\pi^2} \int d^3\Omega D_{M,M}^J(\Omega)^* \hat{R}(\Omega). \quad (24)$$

The normalization factor has been determined by using (23)-(24):

$$N_{J,-M}^2 = \left( \frac{2J+1}{8\pi^2} \right)^2 (\langle B|P_{JM}|B\rangle)^{-1}. \quad (25)$$

Finally, the coefficients  $C_J$  in eq. (18) are given by the expression:

$$\begin{aligned} C_J^2 &= \langle B|P_{JM}|B\rangle \\ &= \frac{2J+1}{8\pi^2} \int d^3\Omega D_{M,M}^J(\Omega) \langle B|\hat{R}(\Omega)|B\rangle. \end{aligned} \quad (26)$$

Once we obtain the projected state, we proceed to evaluate the corresponding energy. Basically we need to calculate the expectation value of the Hamiltonian on the projected state given by (23). The projected energy can be written as:

$$\begin{aligned} E_J &= \langle JM - M | : H : | JM - M \rangle \\ &= 4\pi \int r^2 dr (E_{int} + E_{kin,Q} + E_{J,\sigma} + E_{J,\pi} \\ &\quad + E_\omega + E_{J,\rho} + E_{J,A} + E_{J,pot}) \end{aligned} \quad (27)$$

More details about the projection technique and the evaluation of the each term in the energy can be found in [11, 29].

##### A. Projected observables

The formalism needed to compute most of the observables can be found in [11, 29]. The only quantity for which we need to provide a new explicit expression is the potential energy, since in our potential there is a logarithmic term, not present in the  $\sigma$  model.

The matrix element for which we need to develop a full calculation is:

$$E_{J,pot} = \langle JM - M | : \int d^3r V(\sigma_h, h) : | JM - M \rangle \quad (28)$$

More details about the calculation of this term are given in Appendix II.

To compute the static observables we have used the explicit formulae given in the Appendix of Ref. [29]; in addition to radii and magnetic moments we also show the results for the average number of pions in the projected state, given by:

$$\langle N_\pi \rangle_J = \overline{N}_\pi C_0(J, \overline{N}_\pi), \quad (29)$$

where  $C_0(J, \overline{N}_\pi)$  [11] is a projection coefficient depending on the spin and on the average number of pions  $\overline{N}_\pi$  in the unprojected state. As already mentioned before, we do not perform a projection on the linear momentum, but we adopt an easier approach [30] which provides a rough estimate of the center-of-mass corrections to the baryon total energy. The masses for the  $N$  ( $J = 1/2$ ) and for the  $\Delta$  ( $J = 3/2$ ) are then given by:

$$M_J = (E_J - \mathbf{P}^2)^{1/2}. \quad (30)$$

## V. WIGNER-SEITZ APPROXIMATION TO NUCLEAR MATTER

In order to describe a soliton system at finite density we use the Wigner-Seitz approximation. This approach is very common and it has already been widely applied to both non-linear [14, 15, 19] and linear- $\sigma$  models [18]. Specifically, the Wigner-Seitz approximation consists of replacing the cubic lattice by a spherical symmetric one where each soliton sits on a spherical cell of radius  $R$  with specific boundary conditions imposed on fields at the surface of the sphere. The configuration of the meson fields, centered at each lattice point, generates a periodic potential in which the quarks move.

The spinor of quark fields must satisfy the Bloch theorem:

$$\psi_{\mathbf{k}}(r) = e^{i\mathbf{k}\cdot\mathbf{r}} \Phi_{\mathbf{k}}(r), \quad (31)$$

where  $\mathbf{k}$  is the crystal momentum (which for the ground state is equal to zero) and  $\Phi_{\mathbf{k}}(r)$  is a spinor that has the same periodicity of the lattice.

### A. Boundary conditions

In the literature various sets of possible boundary conditions have been discussed [18, 19]. In our work we adopt the choice of Ref. [18] which relates the boundary conditions at  $R$  to the parity operation,  $\mathbf{r} \rightarrow -\mathbf{r}$ . Respect to this symmetry the lower component  $v(r)$  of quark spinor, the pion  $h(r)$  and the rho  $\rho(r)$  are odd, and therefore they have to vanish at  $R$ :

$$v(R) = h(R) = \rho(R) = 0. \quad (32)$$

Similarly, for the  $\sigma$  field, the upper Dirac component, the  $\omega$  and the  $A$  fields the argument based on parity provides the conditions:

$$u'(R) = \sigma'_h(R) = \omega'(R) = A'_S(R) = A'_T(R) = 0. \quad (33)$$

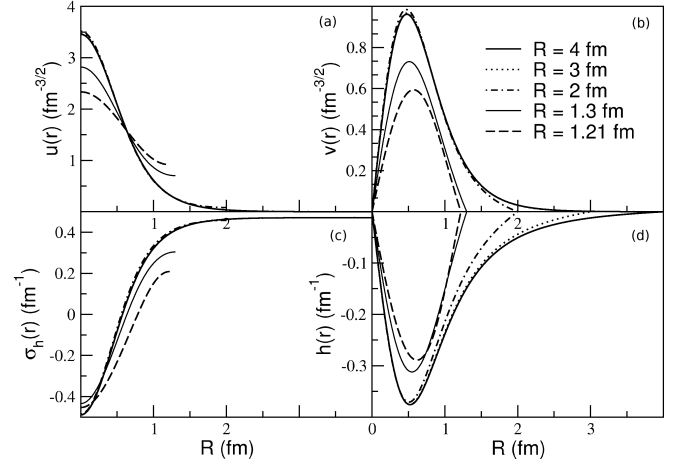


Figure 2. Upper and lower components of the Dirac spinor ((a), (b)),  $\sigma$  and pion fields ((c), (d)), in the model without vector mesons, as functions of the cell radius  $R$ .

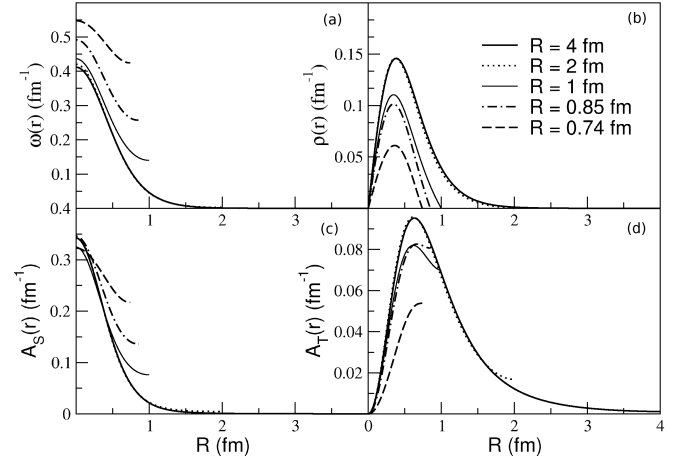


Figure 3. Vector mesons fields, as functions of the cell radius  $R$ . In (a) we plot the  $\omega$  field, in (b) the  $\rho$  field, in (c) the  $A_S$  field and in (d) the  $A_T$  field.

The boundary conditions at  $r = 0$  remain the ones given in eq. (19). Basically the calculation consists in solving the set of coupled field equations in a self-consistent way for a given value  $R$ ; practically we start from  $R = 4$  fm, for which the periodic solutions are indistinguishable from the vacuum ones, and we slowly decrease the cell radius down to the smallest radius for which self-consistent solutions can be obtained. The parameter set is the same used for vacuum calculations.

In Fig. 2 we plot the Dirac and the chiral fields in the model without vector mesons for different values of  $R$ ; down to  $R = 2$  fm, the solutions do not change significantly, but as the cell radius shrinks to lower values, we see that all the fields are deeply modified by the finite density.

For the model including vector mesons, we present in Fig. 3 the trend of the vector mesons fields. To better

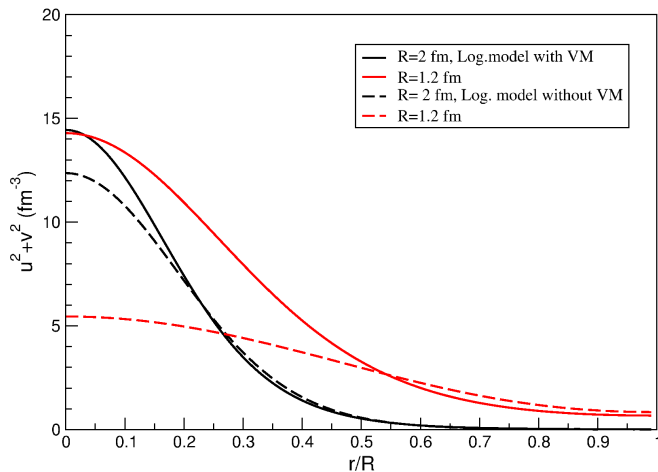


Figure 4. Color online. Baryon density as a function of the ratio  $r/R$  for the model without (dashed line) and with vector mesons (solid line). Two values of the cell radius  $R$  are shown, namely  $R = 2$  fm and  $R = 1.2$  fm.

clarify the difference between the models without and with vector mesons, in Fig. 4 we show the baryon density profiles in the two cases. The relevant feature is that in the model without vector mesons the shape of the soliton becomes significantly more flat, at large densities, than in the case with vector mesons. This effect is due to the repulsion between the two solitons provided by the  $\omega$  field, which prevents the baryon density to become large in the inter-nucleon region. This feature will have an important consequence on the dependence of the radii on the density, as discussed in Sec VII B.

### B. Band width

We are solving a problem in which quarks are moving in a periodic potential and therefore Bloch theorem tells us that a band should form. How to define the width of the band is highly not trivial. The most sophisticated technique is the one provided in [18].

Here we adopt two much simpler procedures. The first method is taken from [15], where the authors estimates the band width as:

$$\Delta = \sqrt{\epsilon_0^2 + \left(\frac{\pi}{2R}\right)^2} - |\epsilon_0|, \quad (34)$$

$$\epsilon_{top} = \epsilon_0 + \Delta, \quad (35)$$

where  $\epsilon_0$  is the eigenvalue of the ground state.

An alternative approximation to the band width is obtained, following [16], by imposing that the lower Dirac component vanishes at the boundary:

$$u(R) = 0. \quad (36)$$

A more accurate evaluation of the band effects can be obtained by solving in a self-consistent way the field

equations, which depend also on  $\mathbf{k}$ , as discussed in [18]. There it is shown that  $\epsilon_{top}$  obtained by imposing the condition (36) is an upper limit to the top of the band and that the true top lies about half way between this upper limit and the bottom of the band. In conclusion, the band width turns out to be considerably smaller than the one estimated using the first method which leads to the upper limit  $\epsilon_{top}$  in eq. (34).

Concerning the filling of the band, when working with chiral solitons at Mean-Field level the relevant quantum number is the grand-spin  $G$  and the lower band corresponds to  $G = 0$ . The only degeneracy remaining is color and therefore the three quarks per soliton are completely filling the band. The total energy of the cell is estimated by assuming a uniform filling and by averaging the energy within the band.

## VI. RESULTS: PROPERTIES OF THE NUCLEON IN VACUUM

We start by showing how the solitonic solutions for the single nucleon can be built and we check that it is possible to provide a reasonable description of the single nucleon properties with the chosen parameter set. In particular we present here results for the lagrangian without vector mesons  $\mathcal{L}_0$  for the set  $m_\sigma = 550$  MeV and the typical value  $g_\pi = 5$  [8, 11]. Instead the parameters for the model with vector mesons are given by  $m_\sigma = 1200$  MeV,  $g_\pi = 3.9$ ,  $g_\omega = 12$  and  $g_\rho = 4$ . This set has been chosen in order to both get saturation at finite density and a reasonable description of the nucleon in vacuum. Anyway, since the calculation of nuclear matter properties done by using the Wigner-Seitz approximation is affected by large uncertainties we also present a second set of results with parameters better fitted to single nucleon properties.

In Tables I and II we present the static properties of the hedgehog baryon at Mean-Field level and we compare them with results obtained in the linear  $\sigma$ -model [22, 31].

In Tables III and IV we show the decomposition of the soliton total energy in its various contributions and again we compare with the linear  $\sigma$ -model [22, 31]. We see that the contributions to the total energy coming from the chiral fields and from the vector mesons are comparable: as expected vector mesons play an important role in the dynamics of the soliton. It is also interesting to notice that the results obtained with the logarithmic model are very similar to the ones obtained with the Mexican hat potential, at zero density, specially when vector mesons are included.

In Tables V and VI we present the results after projection in both models, with and without vector mesons. Moreover, in Table VII we present the results obtained using a second parameter set, better fitted to the single nucleon properties. It is important to remark that our results in the logarithmic model with only chiral fields are consistent with the ones obtained in [20]. There, a different approach based on the coherent pair approxi-

Table I. Various nucleon properties at Mean-Field level in the present work without vector mesons and in the  $\sigma$ -model [31].

Quantity	Log. Model	$\sigma$ -Model	Exp.
$M$ (MeV)	1176	1136	1085
$\langle r_e^2 \rangle_{I=0}$	$(0.76 \text{ fm})^2$	$(0.78 \text{ fm})^2$	$(0.72 \text{ fm})^2$
$\mu_{I=1}$ ( $\mu_N$ )	3.83	3.63	4.70
$\langle r_m^2 \rangle_{I=1}$	$(1.12 \text{ fm})^2$	$(1.14 \text{ fm})^2$	$(0.80 \text{ fm})^2$
$g_A$	1.27	1.22	1.26
$\overline{N}_\pi$	2.4	1.9	/

mation was used. Their results are similar to ours when the coherence length parameter  $x$  is taken to be of the order of one, as suggested in [32].

The results obtained both without and with the vector mesons in general overestimate the experimental values, particularly for the magnetic observables, once the parameters are chosen so that the projected mass of the nucleon is close to its physical value. One has anyway to recall that for the mass an approximate correction for the spurious center of mass motion has been taken into account (see eq. (30)), while no center of mass correction has been done for the other observables. When this further corrections are taken into account the value of some observables typically reduces.

## VII. RESULTS: SOLITONS AT FINITE DENSITY

In this section we present the results obtained by studying a Wigner-Seitz lattice of solitons. We first discuss the energy of the system at finite density and we then present the effect of the density on the single nucleon properties.

Table II. Various nucleon properties at Mean-Field level in the present model and in the  $\sigma$ -model [22] with vector mesons.

Quantity	Log. Model	$\sigma$ -Model	Exp.
$M$ (MeV)	1329.5	1331.7	1085
$\langle r_e^2 \rangle_{I=0}$	$(0.78 \text{ fm})^2$	$(0.76 \text{ fm})^2$	$(0.72 \text{ fm})^2$
$\mu_{I=1}$ ( $\mu_N$ )	4.49	4.51	4.70
$\langle r_m^2 \rangle_{I=1}$	$(0.99 \text{ fm})^2$	$(1.01 \text{ fm})^2$	$(0.80 \text{ fm})^2$
$g_A$	1.34	1.35	1.26
$\overline{N}_\pi$	2.62	2.66	/

Table III. Contributions to the soliton total energy at Mean-Field level in the Logarithmic model and in the Linear  $\sigma$ -model [31]. All quantities are in MeV.

Quantity	Log. Model	Linear $\sigma$ -Model
Quark eigenvalue	83.1	107.4
Quark kinetic energy	1138.0	1056.9
$E_\sigma$ (mass+kin.)	334.5	320.3
$E_\pi$ (mass+kin.)	486.0	373.1
Potential energy $\sigma - \pi$	105.7	120.7
$E_{q\sigma}$	-101.4	-62.3
$E_{q\pi}$	-787.0	-673.2
Total energy	1175.6	1136.2

### A. Energy of the lattice

In Figs. 5 and 6 we present the results of the total energy per unit cell in the present model and in the linear  $\sigma$ -model with and without vector mesons. For each given value of  $m_\sigma$ , the logarithmic model allows the system to reach higher densities. Notice that as  $m_\sigma$  increases, the system remains stable down to lower values of  $R$  because the chiral fields are more and more restricted to lay on the chiral circle. Moreover the introduction of vector mesons

Table IV. Contributions to the soliton total energy at Mean-Field level in the Logarithmic model and in the Linear  $\sigma$ -model with vector mesons [22]. All quantities are in MeV.

Quantity	Log. Model	Linear $\sigma$ -Model
Quark eigenvalue	114.5	112.9
Quark kinetic energy	1075.8	1080.6
$E_\sigma$ (mass+kin.)	213.8	212.2
$E_\pi$ (mass+kin.)	393.2	397.3
Potential energy $\sigma - \pi$	81.2	80.4
$E_\omega$ (mass+kin.)	-194.4	-196.5
$E_\rho$ (mass+kin.)	162.6	165.4
$E_A$ (mass+kin.)	329.5	334.1
$E_{q\sigma}$	6.54	4.74
$E_{q\pi}$	-621.9	-627.1
$E_{q\omega}$	388.9	393.0
$E_{q\rho}$	-163.8	-165.9
$E_{qA}$	-341.8	-346.4
Total energy	1329.5	1331.7

Table V. Projected nucleon properties in the present work without vector mesons and in the linear  $\sigma$ -model and comparison with experimental values.

Quantity	Log. Model	$\sigma$ -Model	Exp.
$E_{1/2} (MeV)$	1075	1002	
$M_N (MeV)$	960	894	938
$E_{3/2} (MeV)$	1140	1075	
$M_\Delta (MeV)$	1032	975	1232
$\langle r_E^2 \rangle_p (fm^2)$	0.55	0.61	0.74
$\langle r_E^2 \rangle_n (fm^2)$	-0.02	-0.02	-0.12
$\langle r_M^2 \rangle_p (fm^2)$	0.7	0.72	0.74
$\langle r_M^2 \rangle_n (fm^2)$	0.72	0.75	0.77
$\mu_p (\mu_N)$	2.25	2.27	2.79
$\mu_n (\mu_N)$	-1.97	-1.92	-1.91
$g_a$	1.52	1.10	1.26
$\langle N_\pi \rangle_J$	1.6 ( $J = 1/2$ )	1.2 ( $J = 1/2$ )	/
	2. ( $J = 3/2$ )	1.6 ( $J = 3/2$ )	

stabilises even more the solution, hence in comparison to the model with only  $\sigma$  and  $\pi$  we can reach higher densities.

In Fig. 8 we plot the quark eigenvalue for the model without vector mesons as a function of the cell radius  $R$ . The line labeled  $\epsilon_{top}^{(a)}$  corresponds to the estimate of the top of the band given by eq. (34), while  $\epsilon_{top}^{(b)}$  follows from eq. (36). It is clear that in absence of vector mesons we never obtain saturation. Moreover to change the value of  $m_\sigma$  does not modify this result. In Fig. 9 we show the analogous results in the case with vector mesons. The band structure is similar to the one in Fig. 8, but here the main difference is given by a significant increase of the top of the band at high densities which allows us to obtain saturation.

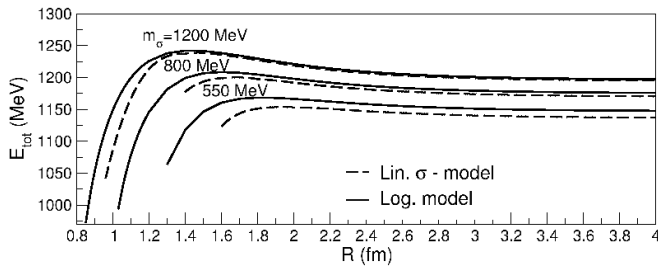


Figure 5. Total energy of the soliton as a function of cell radius  $R$  for the linear  $\sigma$ -model [18] and for the present model without vector mesons. Different values of  $m_\sigma$  are considered,  $g_\pi = 5$ ,  $g_\omega = 12$  and  $g_\rho = 4$ .

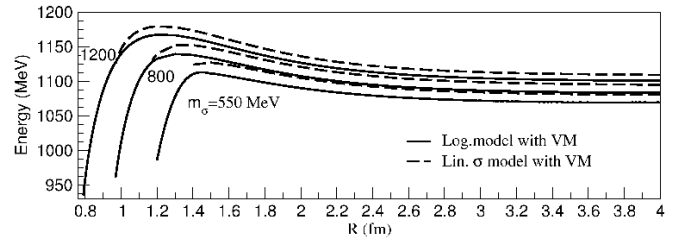


Figure 6. Total energy of the soliton as a function of cell radius  $R$  for the linear  $\sigma$ -model [18] and for the present model with vector mesons. Different values of  $m_\sigma$  are considered.

To better understand our result which indicates the possibility of getting saturation, in Fig. 7 we compare the total energy of the soliton at Mean-Field without the contribution associated with the band. In order to emphasize the effect of the density on the energy we subtracted the mass of the nucleon in vacuum. It is clear that the exchange of vector mesons plays a crucial role, by contributing  $\sim 100$  MeV at  $R = 1$  fm, but it is not sufficient to get saturation. To determine which ingredients of the model are actually providing the repulsion at high densities, in Fig. 10 we plot the interaction energies for each term contributing to the total energy at finite density. The plotted quantities are defined as the value of the chosen energy contribution at  $R$  minus the

Table VI. Projected nucleon properties in the present work and in the linear  $\sigma$ -model with vector mesons and comparison with experimental values.

Quantity	Log. Model	$\sigma$ -Model	Exp.
$E_{1/2} (MeV)$	892	882	
$M_N (MeV)$	763	750	938
$E_{3/2} (MeV)$	1030	1029	
$M_\Delta (MeV)$	918	917	1232
$\langle r_E^2 \rangle_p (fm^2)$	0.59	0.58	0.74
$\langle r_E^2 \rangle_n (fm^2)$	-0.03	-0.02	-0.12
$\langle r_M^2 \rangle_p (fm^2)$	0.69	0.69	0.74
$\langle r_M^2 \rangle_n (fm^2)$	0.70	0.71	0.77
$\mu_p (\mu_N)$	2.72	2.71	2.79
$\mu_n (\mu_N)$	-2.49	-2.5	-1.91
$g_a$	1.6	1.48	1.26
$\langle N_\pi \rangle_J$	1.1 ( $J = 1/2$ )	1.8 ( $J = 1/2$ )	/
	1.3 ( $J = 3/2$ )	2.2 ( $J = 3/2$ )	



Table VII. Projected nucleon properties in the present work and in the linear  $\sigma$ -model with vector mesons and comparison with experimental values for the parameter set:  $g = 3.6$ ,  $g_\omega = 13$ ,  $g_\rho = 4$  and  $m_\sigma = 1200$  MeV.

Quantity	Log. Model	$\sigma$ -Model	Exp.
$E_{1/2}$ (MeV)	1020	1008	
$M_N$ (MeV)	926	912	938
$E_{3/2}$ (MeV)	1148	1147	
$M_\Delta$ (MeV)	1066	1063	1232
$\langle r_E^2 \rangle_p$ (fm <sup>2</sup> )	0.67	0.66	0.74
$\langle r_E^2 \rangle_n$ (fm <sup>2</sup> )	-0.05	-0.05	-0.12
$\langle r_M^2 \rangle_p$ (fm <sup>2</sup> )	0.77	0.76	0.74
$\langle r_M^2 \rangle_n$ (fm <sup>2</sup> )	0.78	0.77	0.77
$\mu_p$ ( $\mu_N$ )	2.63	2.64	2.79
$\mu_n$ ( $\mu_N$ )	-2.37	-2.38	-1.91
$g_a$	1.58	1.46	1.26

corresponding vacuum value:

$$\tilde{E}_i(R) = E_i(R) - E_i(\infty). \quad (37)$$

From the figure it is clear that the band effect strongly influences the total energy of the soliton, by providing the largest contribution to repulsion at high densities. This is not surprising, because the band is associated with the sharing of quarks between nucleons. It is well known [33, 34] that in calculations of the  $N - N$  potential based on quark models the short-range repulsion is associated with the formation of a six-quark bag. In

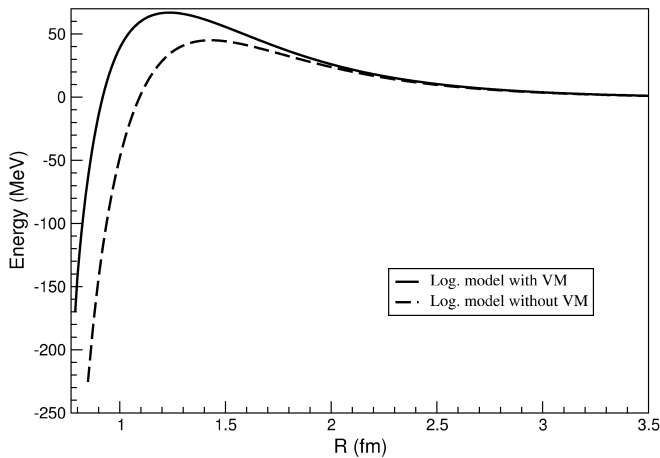


Figure 7. Total energy of the soliton at Mean-Field level in the logarithmic model without vector mesons (dashed line) and with vector mesons (solid line). The parameter values are:  $m_\sigma = 1200$  MeV,  $g_\pi = 5$ ,  $g_\omega = 12$  and  $g_\rho = 4$ .

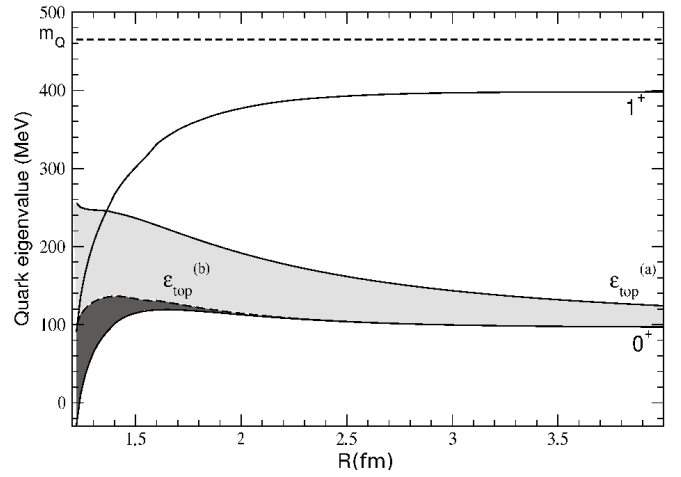


Figure 8. Quark eigenvalue as a function of the cell radius  $R$ , in the model without vector mesons. The shaded areas represent the band as estimated in eq.(34) and in eq. (36). The first excited state  $1^+$  is also shown. The quark mass in vacuum, here 465 MeV, is indicated by the dashed line.

our calculation the exchange of vector mesons is the dominant effect at densities up to  $\rho_0$ , but at very high densities the band effect dominates. The total amount of these contributions leads to the repulsive mechanism responsible for the steep rising of the total energy at high densities, as it can be seen in the upper panel of Fig. 9.

In Figs. 11 and 12 we show in details all the contributions to the total energy (without the band effect). It is clear that the  $\omega$  meson provides short-range repulsion, partially compensated by the interaction of the quarks with the  $A$  meson.

It has been discussed in the literature how to interpret the results obtained using the Wigner-Seitz lattice and in particular which should be the indications of quark deconfinement. In [15] it has been suggested that deconfinement takes place when the upper band, which corresponds to Grand Spin  $G = 1$ , merges with the lower band. In the case with vector mesons this occurs roughly at densities slightly larger than the saturation density. We should keep in mind that the estimate of the width of the band is affected by large uncertainties and it is well possible that in a more refined calculation saturation density and deconfinement density turn out to be well separated.

Which conclusions can be drawn from our analysis? First and foremost we have a scenario in which it is possible, for the first time, to obtain saturation by making use of the rather common idea of getting attraction from the chiral fields and repulsion from the vector fields. In this game the logarithmic potential plays a crucial role, by allowing the solitons to remain stable at densities large enough that the vector mesons can play a role. It is important at this point to clarify whether we can get this

result only in a special and tiny parameters' range or if the mechanism leading to saturation is rather stable respect to the choice of the parameters' values. This analysis is shown in Fig. 13 where we plot the value of the total energy, including the band effects, at the "saturation density" point minus the energy in vacuum for different values of the parameters, at fixed  $m_\sigma = 1200$  MeV. Here "saturation density" means the density at which a local minimum in the total energy appears, even if that minimum is not the global one. The minimum is global when the energy plotted in Fig. 13 is negative and in that situation we are getting real saturation. Instead, when the plotted energy is positive the local minimum corresponds to a sort of metastable state. Since our calculation is affected by large uncertainties we think it is interesting to show also the parameters leading to this "false" minimum, because in a more sophisticated calculation (based for instance on a better estimate of the band) those energies could easily become negative. For parameters' values significantly outside the indicated range no local minimum exists. For instance for values of  $g_\omega > 12$  the local minimum of the energy disappears because the energy keeps raising as the density increases, while for small values of  $g_\omega$  the repulsion cannot contrast the attraction and the energy gets smaller and smaller at large densities. It is important to notice that the range of parameters' values providing "saturation" is at least in part overlapping with the range of parameters' values for which a reasonable description of the single soliton in vacuum can be obtained. Finally, we have to recall that we are not really studying nuclear matter, but rather  $G = 0$  matter, which is composed of degenerate nucleons and deltas. Obviously, no experimental data exist for

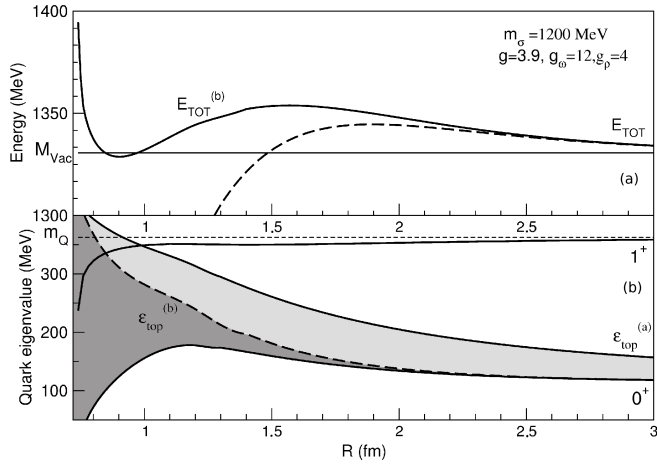


Figure 9. Panel (a): total energy of the soliton with band effects (solid line) and without band effects (dashed line) as a function of the cell radius  $R$  for the model with vector mesons. Panel (b): the quark eigenvalue as a function of the cell radius  $R$  for the model with vector mesons. The shaded areas represent the band as estimated in eq.(34) and in eq. (36). The quark mass, here 362.7 MeV, is indicated by the dashed line.

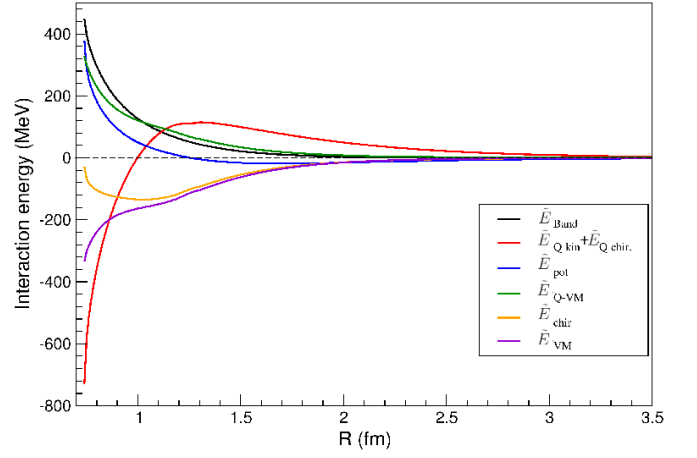


Figure 10. Color online. Interaction energies  $\tilde{E}_i$ , as defined in text, as a function of the cell radius  $R$  in the model with vector mesons. Parameters as in Fig. 9.

that type of theoretical matter, but we can expect it to be saturating, probably with a larger saturation energy than that of nuclear matter. The corresponding saturation density is also obviously unknown.

## B. Nucleon properties at finite density

The question about the modification of the nucleon properties at finite density have been investigated in many analysis, both experimental [35] and theoretical [26, 36–39]. In Figs. 14 and 15 we show how the values of a few observables evolve as a function of the spherical cell density  $\rho_C = (4\pi R^3/3)^{-1}$ . The Mean-

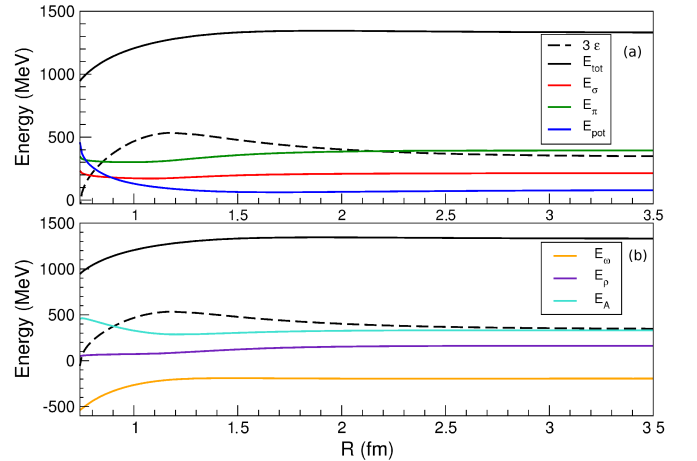


Figure 11. Color online. Panel (a): contributions of the chiral fields to the total energy of the soliton as a function of the cell radius  $R$  in the model with vector mesons. Panel (b): contributions of the vector meson fields to the total energy of the soliton as a function of the cell radius  $R$ . Parameters as in Fig. 9.

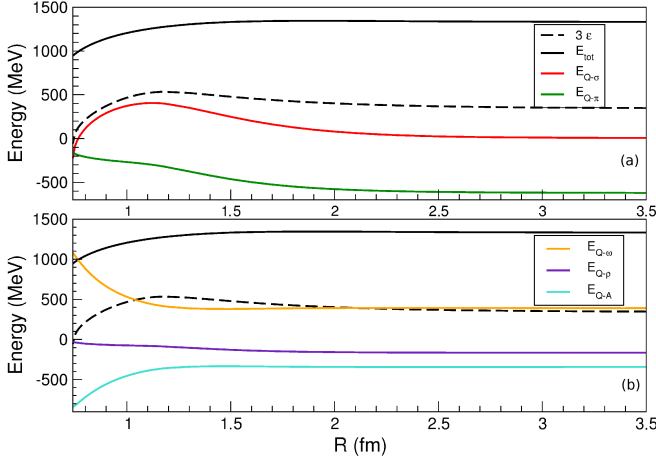


Figure 12. Color online. Panel (a): interaction energies of the chiral fields with quarks as a function of the cell radius  $R$  in the model with vector mesons. Panel (b): interaction energies with the vector mesons as a function of the cell radius  $R$ . Parameters as in Fig. 9.

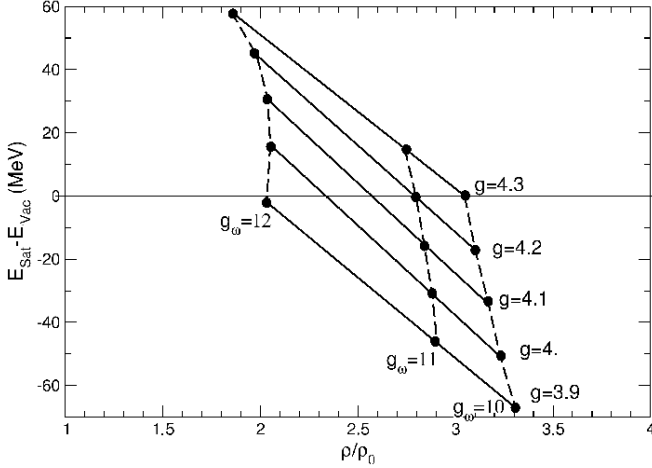


Figure 13. Minimum of the total energy as a function of the density. Different sets of couplings are shown, for which the model admit saturation. See the text for more details.

Field observables evaluated as a function of the density cell are the isoscalar electric and the isovector magnetic radius and the number of pions. The formulae for these quantities for the model without and with vector mesons read [29, 40]:

$$\begin{aligned} \langle r_E^2 \rangle_{I=0} &= \int r^4 (u^2 + v^2) dr \\ \langle r_M^2 \rangle_{I=1} &= \frac{1}{\mu_{I=1}} \int r^5 \frac{2\pi}{9} (G_M^Q + G_M^\pi + G_M^\rho + G_M^A), \end{aligned} \quad (38)$$

and  $\mu_{I=1}$  and the radial functions  $G_m^{field}$  are given in Appendix III. The problem with our evaluation is that in the Wigner-Seitz approach we are forcing a unit of baryon number in every cell of the lattice. Therefore, at densities

large enough that the fields start occupying most of the cell and their value is no more strongly varying inside the cell, the various radii all simply scale with the size of the cell. The results we are obtaining are therefore indicative only at densities low enough that the fields are still relatively well contained inside each cell. As shown in Figs. 2 and 3 all the fields are well confined up to values of density close to  $\rho_0$ . This implies that the behaviour of the observables, evaluated from these fields, have no physical relevance at densities of the order or above nuclear matter saturation density  $\rho_0$ .

The problem we are facing is deeply associated with the Wigner-Seitz approximation in which the effect of the finite density to the various observables is due only to Hartree contributions. In the real case two neighboring nucleons interact also via the Fock term. Notice that at densities large enough that the field fluctuations are suppressed, the Hartree contributions associated e.g with the pion field vanishes. On the contrary the Fock term becomes relevant at those densities and it provides contributions to the electromagnetic observables which in nuclear physics are sometimes called pion-in-flight. These terms, of course, cannot be evaluated in the Wigner-Seitz approach.

Another problem with the Wigner-Seitz approach is that it imposes spherical boundary conditions on the fields. This is particularly dangerous in the case of the chiral fields, since at Mean-Field level directions in ordinary space are connected with directions in isospin space, a situation which is certainly quite far from reality. Due to these problems a work is in progress [41] in which a real lattice will be studied, with boundary conditions which can change depending on the direction. We think it is nevertheless worthy to present our results in Figs. 14-15 so to compare them with future more precise estimates.

For the model containing  $\sigma$  and  $\pi$  only, our results can be meaningful at low densities where the dynamics is dominated by chiral fields. The introduction of vector mesons affects in quite a interesting way the isoscalar radius: as shown in Fig. 4, the repulsion provided by the  $\omega$  field, for densities smaller than  $\rho_0$ , prevents the swelling of the nucleons. The qualitative effect of the inclusion of the vector mesons is to stabilize the shape of the solitons respect to compression. This can be seen also in the case of the magnetic radius where the reduction of this quantity as a function of the density is less marked than in the case without vector mesons. It is also possible to evaluate the so-called "super-ratio" defined as  $(G_E/G_M)^\rho / (G_E/G_M)^{vac}$ , where  $G_{E,M}$  are the electric and magnetic form factors. In our calculation we obtain a reduction of this quantity as a function of the density, similarly to what obtained in other works, although the effect here is much larger. Let us stress again that although the model with vector mesons allows to reach much larger densities, we do not attribute too much significance to the behaviour of the observables at  $\rho \gtrsim \rho_0$  for the reasons explained above. In the lowest panel of Figs. 14 and 15 we also show the behaviour of the number

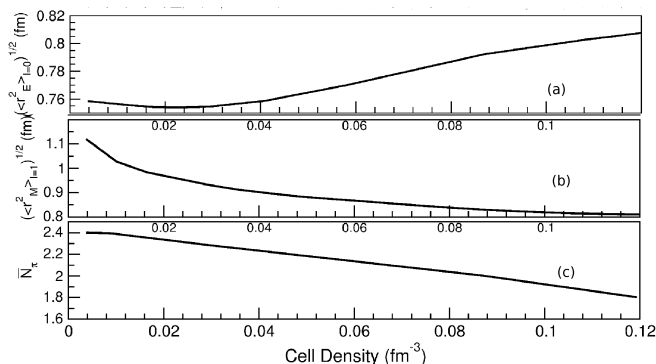


Figure 14. Isoscalar electric radius (panel (a)), isovector magnetic radius (panel (b)) and average number of pions (panel (c)) as a function of cell density  $\rho_C$  for the model without vector mesons.

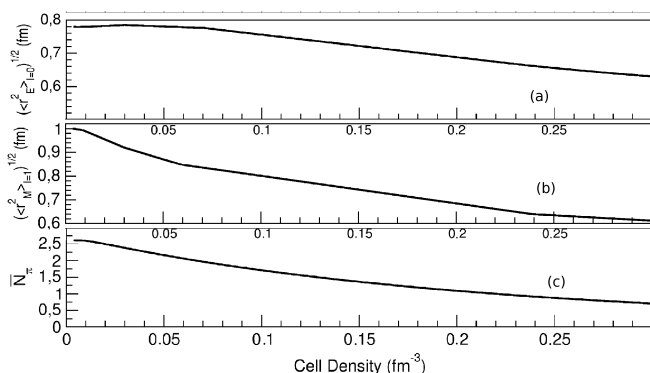


Figure 15. Isoscalar electric radius (panel (a)), isovector magnetic radius (panel (b)) and average number of pions (panel (c)) as a function of cell density  $\rho_C$  for the model with vector mesons.

of pions  $\bar{N}_\pi$  per unit cell at finite density. The possibility of an enhancement of the pion cloud, when the nucleon is not isolated, has been discussed in the literature [37]. In the present approach we obtain instead a decrease of  $\bar{N}_\pi$ . This result stems from the behaviour of the pionic field on the Wigner-Seitz lattice as shown in Fig. 2. The strong reduction of the pionic field is due to the boundary conditions requested by the spherical symmetry. It will be interesting to see if this result survives when a real lattice is used in the calculation.

## VIII. CONCLUSIONS

We used a Lagrangian with quarks degrees of freedom based on chiral and scale invariance to study how the soliton behaves in vacuum and at finite density. We presented results for the simple model with just chiral fields and also for the model including vector mesons. To describe the single nucleon properties in vacuum we have used a projection technique. The values of the static observables in the logarithmic model at zero den-

sity are comparable to the ones obtained using the linear  $\sigma$ -model.

For the description of the soliton at finite density we have employed the Wigner-Seitz approximation. We have shown that the new potential, which includes a logarithmic term originating from the breaking of scale invariance, allows the system, for each given  $m_\sigma$ , to reach densities larger than the ones obtained with the  $\sigma$ -model. Moreover, as expected, the addition of the vector mesons plays a double role in the study at finite density: on one hand it stabilizes the solution and allows to reach even higher densities, on the other hand it partially provides the repulsion necessary to obtain saturation. The remaining repulsive contribution originates from the band effect.

The possibility to obtain saturation seems to be a firm result of the model, at the level of the Wigner-Seitz approximation. In fact, by exploring the space of parameters, we have shown that the interplay between attraction, provided by the chiral fields, and repulsion, given by the omega field and the band effect, allows to get saturation for a rather extended range of parameters' values.

At sub-nuclear densities the dynamics should be dominated by the chiral fields and the modifications of the nucleon observables obtained in our work can therefore be physically relevant in the low-density range. In particular the isoscalar radius presents a slight swelling, of the order of 5% in the model without vector mesons and at even smaller dependence on the density in the complete model. This trend is in agreement with previous calculations [36, 39, 42].

The present work will be extended in several directions. First a more precise and accurate calculation of the band in the soliton crystal will be done following Ref. [18]. Work is in progress in order to study this same model by using the technique developed in Ref. [43], which provides a more precise description of a multi-soliton system. Finally, the model can also be studied at finite temperature, including the dynamics of the dilaton field. We can expect that the effect of the finite temperature on the soliton lattice will be to reduce the stability, by lowering the value of the dilaton field and therefore making it more easy for the chiral fields to fluctuate. It will be interesting to compare the obtained phase diagram with the one proposed by McLerran and Pisarski [10].

## ACKNOWLEDGMENTS

It is a pleasure to thank B.Y.Park and V. Vento for many stimulating discussions, M.Birse and J.McGovern for useful comments and tips on calculations.

## APPENDIX I

In this Appendix we provide the explicit expression for the energy density at Mean-Field given in eq. (21). The quark-mesons interaction and the quark kinetic energies are:

$$E_{int} = \frac{3}{4\pi} \left\{ g_\pi \sigma_h (u^2 - v^2) + 2g_\pi h u v + \frac{g_\omega}{3} \omega (u^2 + v^2) - 2g_\rho \rho u v + g_\rho \left[ \frac{3}{2} A_S \left( u^2 - \frac{1}{3} v^2 \right) + \frac{2}{3} v^2 A_T \right] \right\} \quad (\text{A.39})$$

$$E_{kin,Q} = \frac{3}{4\pi} \left( u \frac{dv}{dr} - v \frac{du}{dr} + \frac{2}{r} u v \right) \quad (\text{A.40})$$

and the energy density of the mesons fields and of the potential read:

$$E_\sigma = \frac{\beta}{2} \left[ -\frac{d\sigma_h}{dr} - g_\rho h \left( A_S + \frac{2}{3} A_T \right) \right]^2 \quad (\text{A.41})$$

$$E_\pi = \frac{\beta}{2} \left[ \frac{dh}{dr} + g_\rho \sigma_h \left( A_S + \frac{2}{3} A_T \right) \right]^2 + \beta \left[ -\frac{h}{r} + g_\rho h + g_\rho \sigma_h \left( A_S - \frac{1}{3} \right) \right]^2 \quad (\text{A.42})$$

$$E_\omega = -\frac{1}{2} \left( \frac{d\omega}{dr} \right)^2 - \frac{1}{2} m_\omega^2 \omega^2 \quad (\text{A.43})$$

$$E_\rho = \left[ \frac{d\rho}{dr} + \frac{\rho}{r} - g_\rho \left( A_S + \frac{2}{3} A_T \right) \left( A_S - \frac{1}{3} A_T \right) \right]^2 + \frac{1}{2} \left[ \frac{2}{r} \rho - g_\rho \rho^2 - g_\rho \left( A_S - \frac{1}{3} A_T \right)^2 \right]^2 + m_\rho^2 \rho^2 \quad (\text{A.44})$$

$$E_A = \left[ \left( \frac{dA_S}{dr} - \frac{1}{3} \frac{dA_T}{dr} \right) - \frac{A_T}{r} + g_\rho \rho \left( A_S + \frac{2}{3} A_T \right) \right]^2 + \frac{1}{2} m_\rho^2 \left( 3A_S^2 + \frac{2}{3} A_T^2 \right) \quad (\text{A.45})$$

$$E_{pot} = V(\phi_0, \sigma_h, h) \quad (\text{A.46})$$

## APPENDIX II

In this Appendix we provide a detailed calculation of the expectation value of the logarithmic potential given in eq. (8) between the projected states (see eq. (27)). As already mentioned and shown in [11], terms which do not involve the pion field (such as the quark-pion interaction energy and the  $\sigma$  and quark kinetic energies) are not affected by projection. The main issue is the evaluation of the matrix elements of the chiral fields between rotated and unrotated hedgehog states.

These matrix elements for the sigma field  $\sigma(\mathbf{r})$  are:

$$\langle B | \hat{R}(\Omega)^{-1} \sigma(\mathbf{r})^n | B \rangle = \bar{\sigma}(\mathbf{r})^n \langle B | \hat{R}(\Omega)^{-1} | B \rangle, \quad (\text{A.47})$$

where:

$$\bar{\sigma}(\mathbf{r}) = \frac{1}{2} \left( \sigma(\mathbf{r}) + \hat{R}(\Omega)^{-1} \sigma(\mathbf{r}) \right) \equiv \sigma_h(r). \quad (\text{A.48})$$

In an analogous way, for the pion field the matrix elements become:

$$\langle B | \hat{R}(\Omega)^{-1} \boldsymbol{\pi}(\mathbf{r}) | B \rangle = \bar{\boldsymbol{\pi}}(\mathbf{r}) h(r) \langle B | \hat{R}(\Omega)^{-1} | B \rangle, \quad (\text{A.49})$$

$$\bar{\boldsymbol{\pi}}(\mathbf{r}) = \frac{1}{2} \left( \hat{\mathbf{r}} + \hat{R}(\Omega)^{-1} \hat{\mathbf{r}} \right). \quad (\text{A.50})$$

Since the potential is a function of the pion only through quadratic terms, by using the previous relation we get:

$$\langle B | \hat{R}(\Omega)^{-1} \boldsymbol{\pi}^2(\mathbf{r}) | B \rangle = g(\Omega, \theta, \phi) \langle B | \hat{R}(\Omega)^{-1} | B \rangle, \quad (\text{A.51})$$

$$g(\Omega, \theta, \phi) = \frac{1}{2} h(r)^2 \left( 1 + \hat{\mathbf{r}} \cdot \hat{R}(\Omega)^{-1} \hat{\mathbf{r}} \right),$$

where the function  $g$  depends on Euler angles  $\Omega$  and on the polar and azimuthal angles.

For a generic function  $F$  of the quadratic pionic terms, the following relation holds:

$$\langle B | \hat{R}(\Omega)^{-1} F[\boldsymbol{\pi}^2(\mathbf{r})] | B \rangle = F[g(\Omega, \theta, \phi)] \langle B | \hat{R}(\Omega)^{-1} | B \rangle. \quad (\text{A.52})$$

Therefore the projection of the potential term can be obtained by leaving the pure  $\sigma$  terms unchanged and by replacing the quadratic terms of the pion with the function  $g$  given in eq. (A.51):

$$V(\sigma_h, h, g(\Omega, \theta, \phi)) = \lambda_1^2 (\sigma_h^2 + h^2 g(\Omega, \theta, \phi)) - \lambda_2^2 \ln (\sigma_h^2 + h^2 g(\Omega, \theta, \phi)) - \sigma_0 m_\pi^2 \sigma_h. \quad (\text{A.53})$$

The expectation value of the potential between the projected states, eq. (A.53), becomes:

$$E_{J,pot} = \langle JJ - J | : \int d^3r V(\sigma_h, h, g(\Omega, \theta, \phi)) : | JJ - J \rangle = \frac{1}{N_J} \int_0^\infty r^2 dr \int_0^\pi \sin \theta d\theta \int_0^{2\pi} d\phi \times \int d\Omega^3 D_{J,J}^J(\Omega) V(\sigma_h, h, g(\Omega, \theta, \phi)) \langle B | \hat{R}(\Omega)^{-1} | B \rangle \quad (\text{A.54})$$

where the Wigner function is equal to:

$$D_{J,J}^J(\Omega) = e^{-iJ(\alpha+\gamma)} \left( \cos \frac{\beta}{2} \right)^{2J}. \quad (\text{A.55})$$

Finally, the overlap between rotated and unrotated hedgehog states reads:

$$\langle B | \hat{R}(\Omega)^{-1} | B \rangle = \left( \cos \frac{\beta}{2} \cos \frac{\alpha+\gamma}{2} \right)^3 \times \exp \left( \bar{N}_\sigma + \frac{\bar{N}_\pi}{3} \left( 4 \cos^2 \frac{\beta}{2} \cos^2 \frac{\alpha+\gamma}{2} - 1 \right) \right). \quad (\text{A.56})$$

Here  $\overline{N}_\sigma$ ,  $\overline{N}_\pi$  are the average numbers of  $\sigma$  and  $\pi$  mesons in the hedgehog state and  $N_J$  is a normalization integral; explicit expressions of these quantities can be found in [11, 29].

### APPENDIX III

The Mean-Field approximation for the isovector magnetic moment reads:

$$\mu_{I=1} = \int r^3 dr \frac{2\pi}{9} (G_m^Q(r) + G_m^\pi(r) + G_m^\rho(r) + G_m^A(r)), \quad (\text{A.57})$$

where the radial functions  $G_i^{field}$  are given by:

$$\begin{aligned} G_M^Q(r) &= \frac{3}{\pi} uv, \\ G_M^\pi(r) &= 4\beta \left[ \frac{1}{r} h^2 - g_\rho h \sigma_h \left( A_S - \frac{1}{3} A_T \right) - g_\rho h^2 \rho \right], \\ G_M^\rho(r) &= 4 \left\{ \frac{2}{r} \rho^2 - g_\rho \rho \left[ \rho^2 + \left( A_S - \frac{1}{3} A_T \right)^2 \right] \right\}, \\ G_M^A(r) &= (-1) \left[ 4 \left( A'_S - \frac{1}{3} A'_T - \frac{A_T}{r} \right) \left( A_S + \frac{2}{3} A_T \right) \right. \\ &\quad \left. + 4g_\rho \rho \left( A_S + \frac{2}{3} A_T \right)^2 \right]. \end{aligned} \quad (\text{A.58})$$

For the model without vector mesons, the coupling constant  $g_\rho$  and the meson fields vanish.

- 
- [1] R. J. Furnstahl and B. D. Serot, Phys. Rev. **C47**, 2338 (1993)
  - [2] E. K. Heide, S. Rudaz, and P. J. Ellis, Nucl. Phys. **A571**, 713 (1994)
  - [3] G. W. Carter and P. J. Ellis, Nucl. Phys. **A628**, 325 (1998)
  - [4] G. W. Carter, P. J. Ellis, and S. Rudaz, Nucl. Phys. **A618**, 317 (1997)
  - [5] G. W. Carter, P. J. Ellis, and S. Rudaz, Nucl. Phys. **A603**, 367 (1996)
  - [6] J. Schechter, Phys. Rev. **D21**, 3393 (1980)
  - [7] A. A. Migdal and M. A. Shifman, Phys.Lett. **B114**, 445 (1982)
  - [8] E. K. Heide, S. Rudaz, and P. J. Ellis, Phys. Lett. **B293**, 259 (1992)
  - [9] L. Bonanno and A. Drago, Phys.Rev. **C79**, 045801 (2009)
  - [10] L. McLerran and R. D. Pisarski, Nucl. Phys. **A796**, 83 (2007)
  - [11] M. Birse, Phys.Rev. **D33**, 1934 (1986)
  - [12] S. Kahana and G. Ripka, Nucl.Phys. **A429**, 462 (1984)
  - [13] J. Aichtzelter, W. Scheid, and L. Wilets, Phys.Rev. **D32**, 2414 (1985)
  - [14] B. Glendenning, N. K., Phys. Rev. **C34**, 1072 (1986)
  - [15] D. Hahn and N. K. Glendenning, Phys. Rev. **C36**, 1181 (1987)
  - [16] M. Birse, J. Rehr, and L. Wilets, Phys.Rev. **C38**, 359 (1988)
  - [17] M. Birse, Prog.Part.Nucl.Phys. **25**, 1 (1990)
  - [18] U. Weber and J. A. McGovern, Phys. Rev. **C57**, 3376 (1998)
  - [19] P. Amore and A. De Pace, Phys. Rev. **C61**, 055201 (2000)
  - [20] M. Abu-Shady and M. Rashdan, Phys.Rev. **C81**, 015203 (2010)
  - [21] J. Sakurai, Physical Review Letters **17**, 1021 (1966)
  - [22] M. W. Broniowski, Phys.Rev.D **34**, 849 (1986)
  - [23] S. Gasiorowicz and D. Geffen, Rev.Mod.Phys. **41**, 531 (1969)
  - [24] P. Ko and S. Rudaz, Phys.Rev. **D50**, 6877 (1994)
  - [25] J. R. Smith and G. A. Miller, Phys. Rev. Lett. **91**, 212301 (2003)
  - [26] J. R. Smith and G. A. Miller, Phys. Rev. C **70**, 065205 (Dec 2004)
  - [27] M. Fiolhais, J. Urbano, and K. Goeke, Phys.Lett. **B150**, 253 (1985)
  - [28] J. Rafelski, Phys. Rev. **D16**, 1890 (1977)
  - [29] E. Ruiz Arriola, P. Alberto, J. N. Urbano, and K. Goke, Nucl. Phys. **A591**, 561 (1995)
  - [30] J. Dethier, R. Goldflam, E. Henley, and L. Wilets, Phys.Rev. **D27**, 2191 (1983)
  - [31] M. C. Birse and M. K. Banerjee, Phys.Rev. **D31**, 118 (1985)
  - [32] T. S. T. Aly, J. A. McNeil, and S. Pruess, Phys. Rev. D **60**, 114022 (1999)
  - [33] K. Shimizu, Rept. Prog. Phys. **52**, 1 (1989)
  - [34] A. Faessler, Prog. Part. Nucl. Phys. **36**, 337 (1996)
  - [35] J. Aubert *et al.* (European Muon Collaboration), Phys.Lett. **B123**, 275 (1983)
  - [36] L. S. Celenza, A. Rosenthal, and C. M. Shakin, Phys. Rev. Lett. **53**, 892 (Aug 1984)
  - [37] M. Ericson and M. Rosa-Clot, Phys.Lett. **B188**, 11 (1987)
  - [38] P. Mulders, Phys.Rept. **185**, 83 (1990)
  - [39] D.-H. Lu, K. Tsushima, A. W. Thomas, A. G. Williams, and K. Saito, Phys.Rev. **C60**, 068201 (1999)
  - [40] T. D. Cohen and W. Broniowski, Phys.Rev. **D34**, 3472 (1986)
  - [41] V. M. Sarti, A. Drago, V. Vento, and B.-Y. Park(2012), arXiv:1201.0675 [nucl-th]
  - [42] J. R. Smith and G. A. Miller, Phys.Rev. **C70**, 065205 (2004)
  - [43] B.-Y. Park, H.-J. Lee, and V. Vento, Phys.Rev. **D80**, 036001 (2009)